Aberration-free dynamic focusing with a multichannel micromachined membrane deformable mirror

Lijun Zhu, Pang-Chen Sun, and Yeshaiahu Fainman

We demonstrate aberration-free dynamic focusing with a low-cost 19-channel continuous-surface micromachined membrane deformable mirror (MMDM). A lookup table of the optimum control voltages for various focal lengths is obtained with an adaptive optics algorithm. Diffraction-limited imaging resolution is achieved owing to the capablility of the MMDM for aberration compensation. The measured speed of the MMDM supports dynamic focusing operations at several hundred hertz. Our dynamic focusing approach is shown to function with either monochromatic or broadband optical sources. © 1999 Optical Society of America

OCIS codes: 230.4040, 110.0110.

1. Introduction

Dynamic focusing has applications in areas such as depth scanning for confocal imaging systems, accessing of volumetric and multilayer optical memory systems, as well as autofocusing for telescope imaging systems. Various approaches have been used to implement dynamic focusing; these include utilizing liquid-crystal,[1] electro-optic,[2] or photorefractive devices[3]; piezoelectric diaphragm lenses or mirrors[4]; and electrostatic membrane mirrors.[5] These approaches suffer from such limitations as having slow operation speed, limited focusing range, limited imaging quality, or for some devices, being constrained to operations with monochromatic or polarized light. Existing electrostatic membrane mirrors employ a single electrode to modulate the surface shape of the membrane, thus introducing strong aberrations during the dynamic focusing process owing to boundary effects.[5] In this manuscript, we present a new dynamic focusing approach that provides aberration-free imaging quality and that can be operated with broadband light sources, with a speed up to several hundred Hz. Our approach employs a multichannel continuous-surface micromachined membrane deformable mirror (MMDM), which is a recently developed low-cost and compact deformable mirror device primarily used in adaptive optics applications.[6,7] Diffraction-limited imaging resolution is achieved by employment of an adaptive optics algorithm to obtain ideal shapes of the mirror surface. Controlling the electrostatic forces between the membrane and the multiple control electrodes generates spherical wave fronts corresponding to various focal lengths. The corresponding driving voltages are obtained and stored in a lookup table, which is used for high-speed dynamic focusing with aberration-free imaging.

2. Generation of the Lookup Table

We use a MMDM with 19 active channels and an active aperture of 10 mm in diameter (from OKO Technology). Figure 1(a) shows the schematic diagram of the MMDM and Fig. 1(b) shows its control electrode layout. The MMDM consists of an aluminum-coated silicon nitride membrane with the electrostatic electrodes underneath. The electrostatic forces between the membrane and the electrodes pull down the membrane and modulate its shape. Other studies provide a more detailed description of the MMDM device.[6,7] Because of the nonlinear and coupled response of the MMDM to the electrostatic actuators, we have previously developed an adaptive control algorithm based on experimentally measured mirror shape responses[7]; this algorithm recursively adjusts the driving voltages to compensate for aberrations of a model eye in an adaptive optics system. In this manuscript, we

The authors are with the Department of Electrical and Computer Engineering, University of California San Diego, MS 0407, 9500 Gilman Drive, La Jolla, California 92093-5003. L. Zhu's e-mail address is lzhu@ucsd.edu.

Received 26 February 1999; revised manuscript received 8 June 1999.

0003-6935/99/255350-05$15.00/0

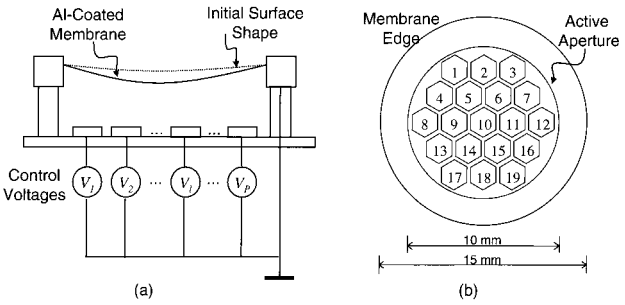

Fig. 1. (a) Schematic diagram and (b) electrode layout of the MMDM.

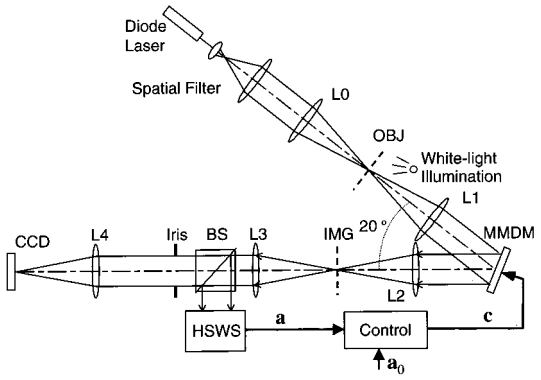

Fig. 2. Experimental setup used to obtain the optimum driving voltages of the MMDM for aberration-free dynamic focusing. All lenses are achromatic doublets.

extend the use of the algorithm to create the desired spherical shapes of the MMDM for dynamic focusing. Our adaptive optics algorithm is based on the measurement of the wave-front error between the ideal wave front $\phi_0(x, y)$ and the actual wave front $\phi(x, y)$ reflected from the MMDM. The wave front $\phi(x, y)$ is measured with a Hartmann–Shack wave-front sensor.[7] The algorithm calculates a small adjustment of the driving voltages that reduces the wave-front error and makes the reflected wave front $\phi(x, y)$ gradually converge to the desired wave front $\phi_0(x, y)$.

The wave front $\phi(x, y)$ is represented by a Zernike polynomial decomposition,[8] described by

$$\phi(x, y) = \frac{2\pi}{\lambda} \sum_{k=1}^{M} a_k z_k(x, y), \tag{1}$$

where λ is the wavelength of light, M is the total number of Zernike polynomials used, $z_k(x, y)$ is the kth Zernike polynomial with a_k being its coefficient. We use wave-front variance σ^2 over the entire aperture of the beam as a measure of the error between $\phi(x, y)$ and $\phi_0(x, y)$,

$$\sigma^2 = \frac{1}{A} \iint_{\text{aperture}} [\phi(x, y) - \phi_0(x, y)]^2 dx dy, \tag{2}$$

where A is the area of the beam aperture. A recursive equation in a matrix form is obtained for iterative adjustment of the driving voltages so that σ^2 is reduced to its minimum. By using a derivation similar to that in Ref. 7, we obtain

$$\mathbf{c}_{\text{new}} = \mathbf{c}_{\text{old}} - 2\mu \mathbf{B}^T[(\mathbf{a} - \mathbf{a}_0)^* \mathbf{w}], \tag{3}$$

where the vector $\mathbf{c} = [V_1^2 V_2^2 \ldots V_P^2]^T$ represents the control voltages $V_l (l = 1, 2, \ldots, P)$ applied to the electrodes of the MMDM with a total of P electrodes (channels); T stands for the transpose operation; μ is a positive scalar representing the convergence rate whose value is determined empirically; $\mathbf{B}$ is a characteristic matrix representing the MMDM response with respect to the driving voltages and can be experimentally measured as described in detail in Ref. 7; vectors $\mathbf{a} = [a_1\ a_2 \ldots a_M]^T$ and $\mathbf{a}_0 = [a_{01}\ a_{02} \ldots a_{0M}]^T$ are Zernike polynomial coefficients, used to represent $\phi(x, y)$ and $\phi_0(x, y)$, respectively; $\mathbf{w}$ is the weighting vector for the Zernike coefficients; and the operator * denotes an element by element multiplication of the two vectors.

For dynamic focusing, the desired function $\phi(x, y)$ is a spherical wave front that corresponds to the spherical term of Zernike polynomials. We use the definition of the Zernike polynomials given by Malacara and DeVore[8] where the fourth term,

$$z_4(x, y) = 2x^2 + 2y^2 - 1,$$

is the desired spherical function. Therefore the desired wave front $\phi_0(x, y)$ is expressed by

$$\phi_0(x, y) = \frac{2\pi}{\lambda} a_{04} z_4(x, y) = \frac{2\pi}{\lambda} [2a_{04}(x^2 + y^2) - a_{04}]. \tag{4}$$

The corresponding focal length f for the wave front $\phi_0(x, y)$ is given by

$$f = \frac{1}{4a_{04}}. \tag{5}$$

For a specific focal length, the Zernike coefficient a_{04} can be calculated with Eq. (5). Then, when the driving voltages (i.e., the vector $\mathbf{c}$) are iteratively adjusted to minimize the wave-front variance using Eq. (3), $\phi(x, y)$ converges to the desired wave front $\phi_0(x, y)$. Repeating the above process yields a lookup table of the optimum driving voltages associated with various focal lengths.

3. Experiments and Results

Figure 2 shows the experimental setup used to obtain the desired shapes of the MMDM for various focal lengths. The MMDM is tilted to separate the incident and the reflected beams by an angle of 20°. The tilt introduces a strong astigmatism in addition to the initial aberrations caused by the imperfection of the MMDM surface itself. These aberrations can be compensated by our adaptive optics algorithm, showing the flexibility of our approach for dynamic focusing. A collimated laser beam is introduced onto the MMDM. Since the MMDM surface can only be de-

Table 1. Focal Lengths, Curvatures, and Root-Mean-Square Variances of the Wave Fronts Reflected from the MMDM

Focal length (m)	−6.5	−7.5	−11.0	−22.5	20.0	10.0	5.0	4.0	3.0
Curvature (1/m)	−0.15	−0.13	−0.09	−0.04	0.05	0.1	0.2	0.25	0.33
σ (wavelengths)	0.14	0.10	0.07	0.05	0.03	0.02	0.03	0.04	0.10

formed to a concave shape, we adjust lenses L0 and L1 to provide a divergent spherical wave bias such that the wave-front error compensation by MMDM can be performed in both directions. The reflected wave front $\phi(x, y)$ is imaged on (with L2, L3, and BS) and analyzed by the Hartmann–Shack wave-front sensor (HSWS in Fig. 2). To achieve dynamic focusing, we first find corresponding values of a_{04} in Eq. (5) and use Eq. (3) for optimum contol of the closed-loop system of Fig. 1. For each focal length, we find optimum driving voltages that minimize the variance σ^2 of Eq. (2) at a laser wavelength of $\lambda = 0.685$ μm. The optimum driving voltages are obtained with 20 Zernike polynomials ($M = 20$) and 19 MMDM control channels ($P = 19$). The results are summarized in Table 1, showing that the focal length of the reflected wave front can be varied in a range from −7.5 to 3.0 m with $\sigma < 0.1$ wavelength, which corresponds to a curvature ranging from −0.13 to 0.33 (1/m). The actual focal range can be modified to suit specific applications by a proper choice of the lenses.

To use our system to observe aberration-free images (Fig. 2), we place an United States Air Force (USAF) resolution target in the plane OBJ illuminated with a white-light source. The aerial image is formed in the plane IMG by lenses L1 and L2 ($f =$ 100 mm) with the MMDM in the Fourier plane to adjust the focus dynamically. It is then imaged onto a CCD camera by lenses L3 and L4 with an iris placed in the conjugate plane of the MMDM to limit the aperture size of the system to the 10-mm diameter of the active area of the MMDM. We obtain and compare two images: Fig. 3(a) is obtained with all electrodes under the same voltage to simulate a single-electrode membrane mirror device, whereas we obtained Fig. 3(b) by driving the MMDM with the optimal voltages from the lookup table. Because of the angle of incidence to the MMDM, significant astigmatism is observed when we apply the same voltage to all the electrodes. Figure 3(a) shows such an image with astigmatism, where only the vertical bars are in focus and the horizontal bars are blurred (see group 5). Using voltages from the lookup table, significantly reduces astigmatism and other aberrations, and both horizontal and vertical bars are in good focus [Fig. 3(b)]. The system can resolve up to group 6-1, corresponding to a line width of 8 μm, which is the Rayleigh resolution limit of our system at a wavelength of 656 nm. The diffraction-limited image is obtained from our imaging setup with white-light illumination. To demonstrate the range of the dynamic focusing, we cut a paper copy of the USAF resolution target into halves, separate them by a distance of 4 mm in depth, and locate them slightly in front of and behind the plane OBJ (Fig. 2). By adjusting the focal length of the MMDM, we are able to focus both halves of the resolution target onto the CCD camera without any movement of the object or the CCD camera. Figure 4 shows the resulting images. The resolution of these images is limited by the resolution of the paper copy of the USAF resolution target.

The speed and the stability of the MMDM are also important issues for dynamic focusing applications.

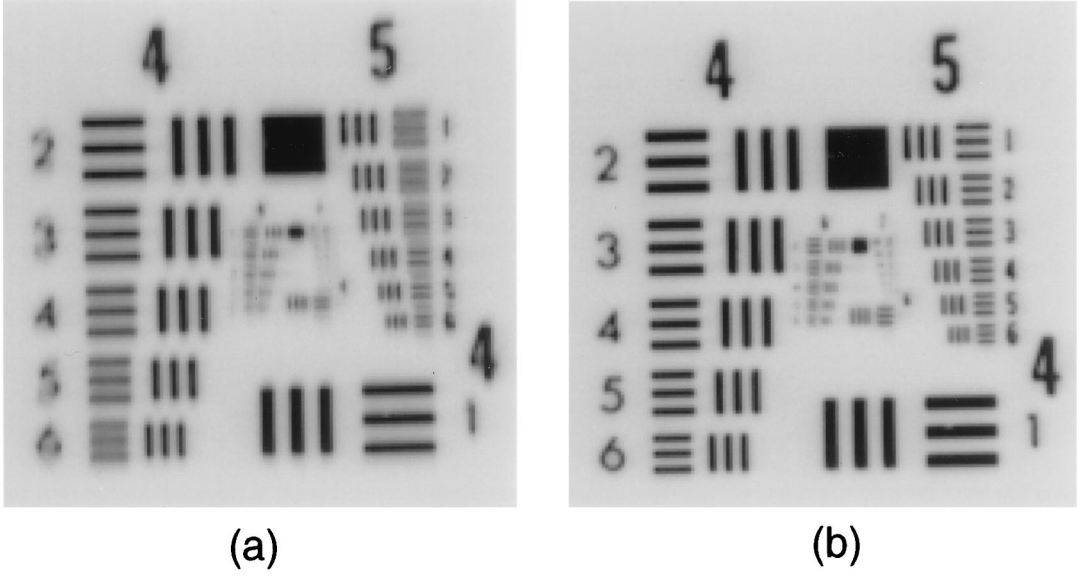

Fig. 3. Images of the USAF resolution target obtained (a) without and (b) with aberration compensation.

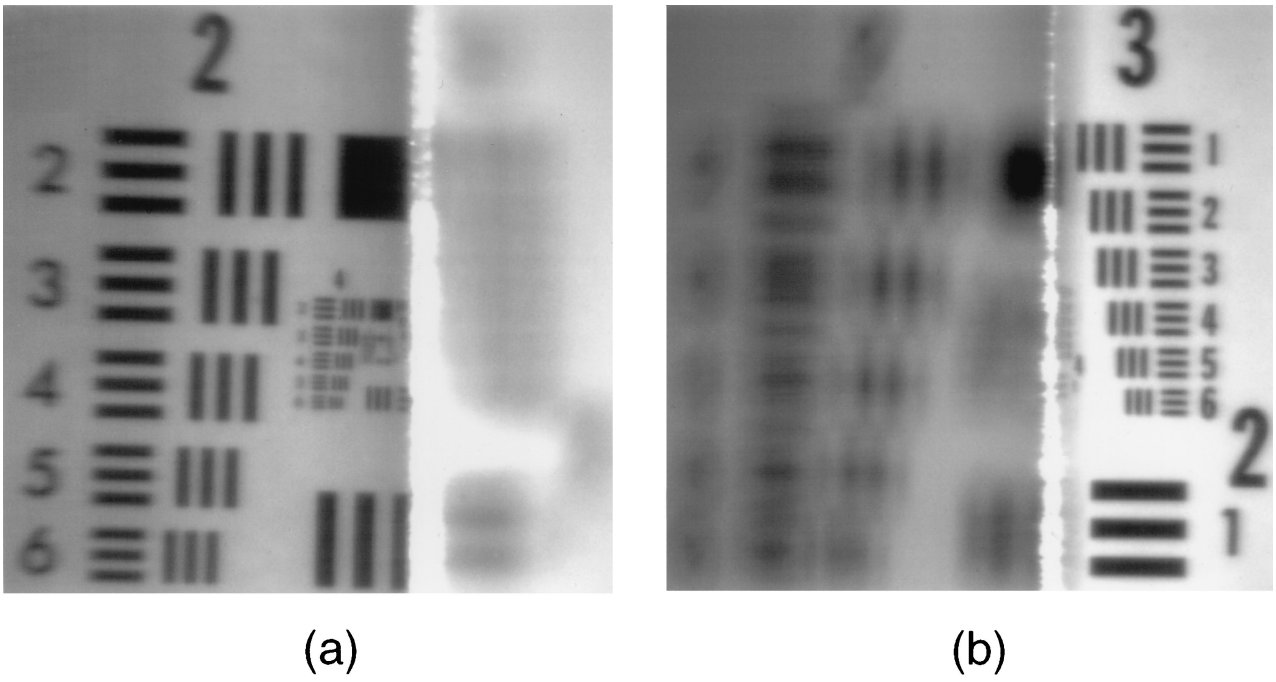

Fig. 4. Dynamic focusing images of both halves of a paper copy of the USAF resolution target separated by a distance of 4 mm in depth.

To measure the time response, we illuminate the MMDM with a laser beam and place a photodetector with a small aperture ($\sim$2 mm^2) near the plane IMG shown in Fig. 2, such that the laser beam is wider than the detector aperture. The MMDM is driven in time by a square waveform between two focal lengths at a frequency of 200 Hz. The detected power follows the time response of the MMDM. Figure 5 shows an oscilloscope trace of the detected intensity versus time as the mirror is switched between two focal states. In switching from one focal length to the other, the mirror first overshoots and then stablizes within approximately 1.3 ms, indicating that a rate of approximately 770 focal states per second is achievable with our MMDM. The speed of the MMDM is limited by the material mechanical property and the dimension of the membrane shown in Fig. 1. To observe the stability of the MMDM over a long period, we measured the wave-front variance every 10 s for an 8-min period while holding the driving voltages from the lookup table constant. The results show a good stability of the mirror with root-mean-square variances σ ranging from 0.018 to 0.025 wavelength.

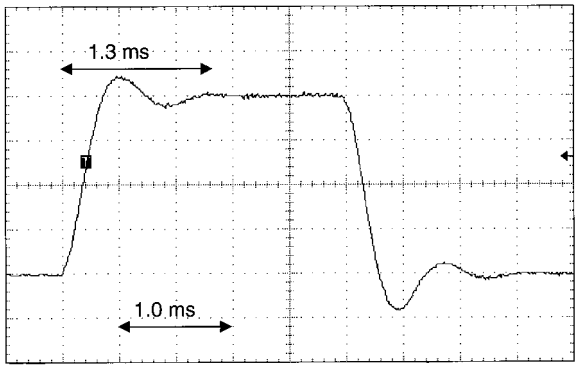

Fig. 5. Time response of the MMDM: Oscilloscope trace of the detected power as the MMDM switchs between two focal lengths at 200 Hz.

4. Conclusions

In summary, we have demonstrated dynamic focusing with significantly reduced aberrations with a low-cost MMDM. The reported aberration-free dynamic focusing system can be used for monochromatic as well as broadband imaging applications. A lookup table of the optimum contol voltages for various focal lengths has been obtained with the adaptive optics algorithm. Diffraction-limited imaging resolution is achieved by aberration compensation. The speed of the MMDM has been measured showing that dynamic focusing at several hundred hertz can be achieved.

This research was supported in part by a grant from the National Science Foundation and the Whitaker Foundation.

References

1. S. T. Kowel, P. Kornreich, and A. Nouhi, "Adaptive spherical lens," Appl. Opt. **23,** 2774–2777 (1984).
2. T. Tatebayashi, T. Yamamoto, and H. Sato, "Electro-optic variable focal-length lens using PLZT ceramic," Appl. Opt. **30,** 5049–5055 (1991).
3. J. Ma, B. Catanzaro, J. E. Ford, Y. Fainman, and S. H. Lee, "Photorefractive holographic lenses and applications for dynamic focusing and dynamic image shifting," J. Opt. Soc. Am. A **11,** 2471–2480 (1994).
4. T. Kaneko, T. Ohmi, N. Ohya, and N. Kawahara, "A compact

and quick-response dynamic focusing lens," Sens. Actuators A, **70,** 92–97 (1998).
5. T. Koumura, T. Kaneko, and T. Hattori, "Aberration reduction of Si diaphragm dynamic focusing mirror," J. Japan Soc. Precis. Eng. **61,** 697–701 (1995).
6. G. Vdovin and P. M. Sarro, "Flexible mirror micromachined in silicon," Appl. Opt. **34,** 2968–2972 (1995).
7. L. Zhu, P.-C. Sun, D.-U. Bartsch, W. R. Freeman, and Y. Fainman, "Adaptive control of a micromachined continuous-membrane deformable mirror for aberration compensation," Appl. Opt. **38,** 168–176 (1999).
8. D. Malacara and S. L. DeVore, "Interferogram evaluation and wavefront fitting," in *Optical Shop Testing*, 2nd ed., D. Malacara, ed. (Wiley, New York 1992), pp. 461–472.